scientific reports

Check for updates

OPEN

Correlation between amide proton transfer-related signal intensity and diffusion and perfusion magnetic resonance imaging parameters in high-grade glioma

Masanori Nakajo[1,3], Manisha Bohara[1,3], Kiyohisa Kamimura[1], Nayuta Higa[2] & Takashi Yoshiura[1]✉

Amide proton transfer (APT) imaging is a magnetic resonance (MR) molecular imaging technique that is sensitive to mobile proteins and peptides in living tissue. Studies have shown that APT-related signal intensity (APTSI) parallels with the malignancy grade of gliomas, allowing the preoperative assessment of tumor grades. An increased APTSI in malignant gliomas has been attributed to cytosolic proteins and peptides in proliferating tumor cells; however, the exact underlying mechanism is poorly understood. To get an insight into the mechanism of high APTSI in malignant gliomas, we investigated the correlations between APTSI and several MR imaging parameters including apparent diffusion coefficient (ADC), relative cerebral blood volume and pharmacokinetic parameters obtained in the same regions-of-interest in 22 high-grade gliomas. We found a significant positive correlation between APTSI and ADC (ρ = 0.625 and 0.490 for observers 1 and 2, respectively; $p < 0.001$ for both), which is known to be inversely correlated with cell density. Multiple regression analysis revealed that ADC was significantly associated with APTSI ($p < 0.001$ for both observers). Our results suggest possible roles of extracellular proteins and peptides in high APTSI in malignant gliomas.

Chemical exchange saturation transfer (CEST) is a novel imaging contrast mechanism in magnetic resonance imaging (MRI)[1]. CEST is based on the physical exchange of protons between solutes and water molecules, which is called chemical exchange. Amide proton transfer (APT) is a specific type of CEST for amide protons in mobile proteins and peptides[2]. APT imaging is considered the most clinically feasible CEST imaging because its specific resonance frequency is remote (3.5 ppm down field) from the water resonance frequency. Studies have shown the potential clinical uses of APT imaging, especially in assessing brain tumors. In diffuse gliomas, several studies have shown that APT-related signal intensity (APTSI) increases with increasing malignancy grades as defined by the World Health Organization (WHO)[3–6]. Moreover, APTSI has been reported as a useful imaging marker in distinguishing recurrent gliomas after chemoradiation therapy from radiation necrosis[7–9], evaluating early response to treatment[10], and predicting prognosis[11]. The most widely accepted hypothesis for higher APTSI in malignant gliomas is that APTSI reflects cytosolic protein that would increase in malignant gliomas with a higher proliferative activity. Nonetheless, extracellular proteins and peptides such as those in fluid-filled cysts and hemorrhage can be sources of APTSI[12,13]. Thus, the underlying mechanism of high APTSI in malignant gliomas is not fully understood. One possible approach to get insight into this mechanism is to investigate the correlations between APTSI and other imaging parameters. This study correlates APTSI with diffusion and perfusion MRI parameters in malignant gliomas.

[1]Department of Radiology, Kagoshima University Graduate School of Medical and Dental Sciences, 8-35-1 Sakuragaoka, Kagoshima 890-8544, Japan. [2]Department of Neurosurgery, Kagoshima University Graduate School of Medical and Dental Sciences, 8-35-1 Sakuragaoka, Kagoshima 890-8544, Japan. [3]These authors contributed equally: Masanori Nakajo and Manisha Bohara. ✉email: yoshiura@m3.kufm.kagoshima-u.ac.jp

Materials and methods

Patients. This retrospective study was approved by the Institutional Review Board (IRB) of Kagoshima University Hospital (approval number: 190103) and the need to obtain informed consent from the patients was explicitly waived by the IRB which approved this study's protocol. The study was performed in accordance with the Declaration of Helsinki. From August 2016 to January 2018, APT-weighted imaging (APTWI) was performed as a part of the preoperative MRI examination protocol for brain tumors in our hospital. In this study, the inclusion criteria were (1) MRI examination including APTWI, diffusion-weighted imaging (DWI), dynamic contrast-enhanced (DCE) imaging, and dynamic susceptibility contrast (DSC) perfusion imaging on the same day within 14 days before surgery and (2) pathological confirmation of high-grade diffuse glioma (either grade III or IV). Statuses of the isocitrate hydrogenase (IDH) mutation and 1p/19q codeletion were determined for each tumor using the Sanger sequencing and fluorescence in situ hybridization, respectively. The following patients were excluded from the study: (1) patients who received any treatment before MRI examination, (2) those with recurrent tumor, and (3) those with severe artifacts that preclude appropriate image analysis.

MRI. All patients underwent MRI examination using a 3.0 T imager (Ingenia, Philips, Best, The Netherlands) and a 15-channel head coil. APTWI was performed using a two-channel parallel transmission scheme with a saturation pulse with a duration of 2 s (40 × 50 ms, sinc-Gauss-shaped elements) and a saturation power level of B1 (rms = 2.0 μT)[14,15] at 25 saturation frequency offsets ranging from − 6 to + 6 ppm with a step of 0.5 ppm and one far-off-resonant frequency (− 1560 ppm) for signal normalization. The other imaging parameters were as follows: fast spin-echo readout with driven equilibrium refocusing; echo train length (ETL) = 128; sensitivity encoding (SENSE) acceleration factor = 1; repetition time (TR) = 3600 ms; echo time (TE) = 4.8 ms; matrix = 128 × 128 (reconstructed to 256 × 256); slice thickness = 5 mm, field of view (FOV) = 230 × 230 mm; and scan time = 2 min and 20 s for one Z-spectrum. A ΔB0 map for off-resonance correction was acquired separately using a 2D gradient-echo with identical spatial resolution for a point-by-point ΔB0 correction[14,15].

DWI was performed using a single-shot spin-echo echo-planar imaging (EPI) sequence using the following imaging parameters: b value = 0 and 1000 s/mm^2; number of diffusion-encoding direction = 3; SENSE acceleration factor = 2.5 (phase); TR = 4250 ms; TE = 63 ms; flip angle (FA) = 90°; number of signals averaged = 2; matrix = 128 × 128 (reconstructed to 256 × 256); number of slices = 24; slice thickness = 5 mm; interslice gap = 1 mm; FOV = 230 × 230 mm; and scan time = 1 min and 40 s.

DCE imaging was performed using a 3D fast field-echo sequence using the following imaging parameters: SENSE acceleration factor = 1.8 (phase) × 1.1 (slice); TR = 6.1 ms; TE = 4.6 ms; FA = 15°; matrix = 128 × 128 (reconstructed to 256 × 256); number of slices = 9; slice thickness = 6 mm; FOV = 230 × 230 mm; and scan time = 5 min and 19 s. Ninety-five dynamic images were obtained at an interval of 3.4 s starting at 30 s before the contrast injection. A power injector (Sonic Shot 7, Nemoto Kyorindo, Tokyo, Japan) was used for intravenous injection of a Gadolinium-based contrast agent (GBCA) (either meglumine gadopentetate or meglumine gadoterate, 0.05 mmol/kg) at a rate of 2 ml/s followed by a saline flush (20 ml, 2 ml/s). A pre-contrast 3D fast filed-echo imaging was performed before the DCE imaging to obtain a pre-contrast T1 value of each voxel using the same imaging parameters as those in the DCE scan, except for an FA of 5°.

DSC perfusion imaging was performed immediately after the completion of DCE imaging using a single-shot field-echo EPI sequence using the following imaging parameters: SENSE acceleration factor = 2.3 (phase); TR = 1610 ms; TE = 40 ms; FA = 75°; matrix = 112 × 112 (reconstructed to 224 × 224); number of slices = 24; slice thickness = 5 mm; interslice gap = 1 mm; FOV = 230 × 230 mm; scan time = 1 min and 41 s. Dynamic imaging was started 8 s before contrast injection. A GBCA (0.05 mmol/kg) was injected at a rate of 4 ml/s followed by a saline flush (20 ml, 4 ml/s).

Post-contrast transverse T1-weighted spin-echo images (T1WIs) were obtained using the following imaging parameters: TR = 410 ms; TE = 10 ms; number of signals averaged = 1; matrix = 304 × 304 (reconstructed to 512 × 512); number of slices = 24; slice thickness = 5 mm; interslice gap = 1 mm; FOV = 230 × 230 mm; and scan time = 2 min and 46 s.

Other standard MRI sequences included pre-contrast T1WI, T2-weighted imaging, fluid-attenuated inversion recovery imaging, susceptibility-weighted imaging, and post-contrast 3D time-of-flight MR angiography; these sequences were not actively used in this study, although pre-contrast T1WIs were used to confirm contrast enhancement.

Generation of parametric maps. The B0 inhomogeneity correction for APT image data was performed using a separately obtained B0 map as previously described. Subsequently, APTWIs were generated using pixel-by-pixel mapping of APTSI, which is defined as the magnetization transfer ratio asymmetry (MTRasym) at 3.5 ppm: MTRasym (3.5 ppm)

$$\begin{aligned} \mathrm{APTSI} &= \mathrm{MTRasym}\left(3.5\ \mathrm{ppm}\right) \\ &= \left[\mathrm{S}\left(-3.5\ \mathrm{ppm}\right) - \mathrm{S}\left(+3.5\ \mathrm{ppm}\right)\right]/\mathrm{S0}, \end{aligned}$$

where S (− 3.5 ppm), S (+ 3.5 ppm), and S0 are the signal intensities obtained at − 3.5 ppm, + 3.5 ppm, and − 1560 ppm, respectively. The APT image analyses were performed using an in-house plug-in software running on ImageJ (v1.47v; National Institutes of Health, Maryland, USA).

Apparent diffusion coefficient (ADC) maps were obtained from the DWI at b values of 0 and 1000 s/mm^2 assuming the mono-exponential signal decay.

Analysis of the DCE images was performed using the extended Tofts model on an image analysis workstation (IntelliSpace Portal, Philips, The Netherlands). The maps of the following four pharmacokinetic parameters were

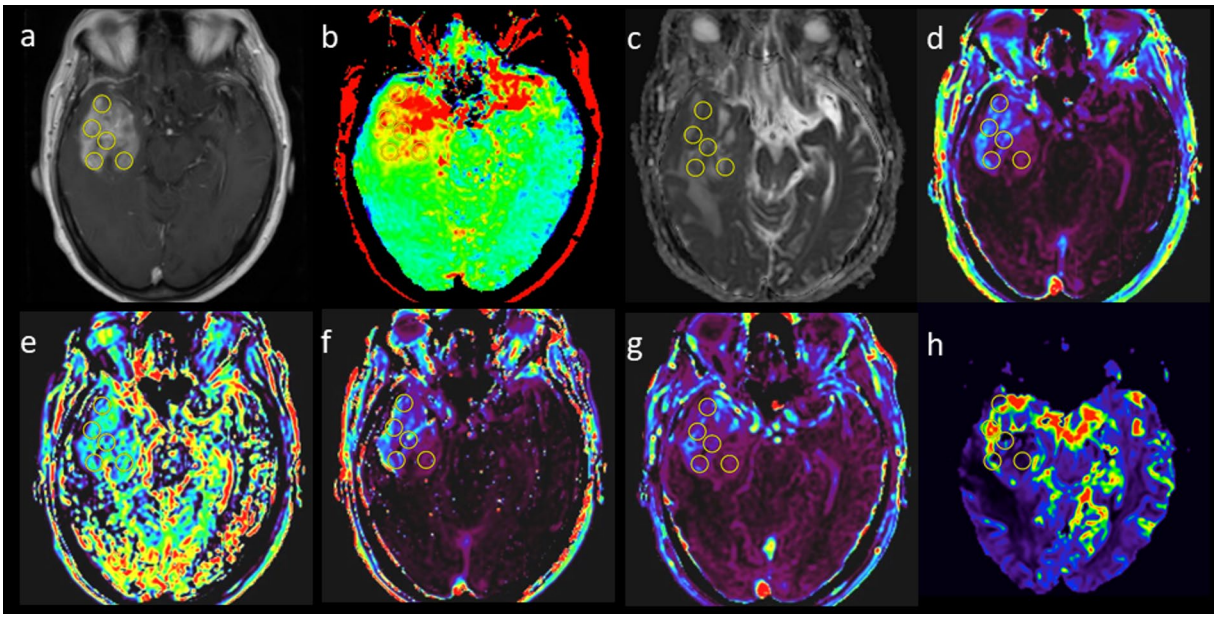

Figure 1. Region-of-interest (ROI) measurements in a 68-year-old female with glioblastoma. Round ROIs with a diameter of 10 mm are placed to fill the solid enhancing part of the tumor on contrast-enhanced T1-weigted image (**a**). The ROIs were copied onto maps of APTSI (**b**), ADC (**c**), K^{trans} (**d**), k_{ep} (**e**), v_e (**f**), v_p (**g**), and rCBV (**h**).

generated: the volume of extravascular extracellular space (EES) per unit volume of tissue (v_e), the blood plasma volume per unit volume of tissue (v_p), the volume transfer constant between blood plasma and EES (K^{trans}), and the rate constant between EES and blood plasma (k_{ep}). While analyzing each tumor, a patient's recent (within 2 weeks) hematocrit and the relaxivity of the administered GBCA (3.8 mM^{-1} s^{-1} for meglumine gadopentetate and 3.4 mM^{-1} s^{-1} for meglumine gadoterate)[16] were input. The arterial input function was automatically obtained.

The DSC perfusion images were analyzed using a commercially available software (IB Neuro 2.0RC; Imaging Biometrics, Elm Grove, WI). Contrast leakage-corrected maps of cerebral blood volume relative to the normal-appearing white matter (rCBV) were automatically obtained.

Region-of-interest analysis. For each patient, maps of APTSI, ADC, pharmacokinetic parameters, and rCBV were co-registered to post-contrast T1WIs with affine transformation using the TurboReg algorithm[17].

Region-of-interest (ROI) analysis was performed by two independent observers with six (observer 1) and three (observer 2) years of experience in neuroradiology. The observers placed round ROIs with a diameter of 10 mm to fill the enhancing solid part of each tumor (Fig. 1, ROIs for the other 21 patients are shown in Supplementary Fig. S1). They placed as many ROIs as possible but were careful to avoid overlaps of ROIs and exclude non-enhancing parts. ROIs were first placed on the post-contrast T1WIs and then copy-and-pasted onto the co-registered parametric maps. The mean value of each parameter was obtained for each ROI. We used relatively large ROIs rather than voxel-by-voxel comparison so that the comparisons between the parameters would be immune to spatial co-registration imperfections.

Statistical analysis. Correlations between the quantitative MR image parameters (APTSI, ADC, K^{trans}, k_{ep}, v_e, v_p, and rCBV) measured in the same ROIs were evaluated using Spearman's rank-correlation test. The contributions of ADC, K^{trans}, k_{ep}, and rCBV to APTSI were analyzed using multiple regression analysis. The v_e and v_p were not included in the independent variables because of their strong correlations with K^{trans} and k_{ep} and rCBV, respectively. *P* values of < 0.05 were used to denote statistical significance. All statistical analyses were performed using Statistical Package for the Social Sciences (version 24.0; IBM Corporation, Armonk, NY, USA).

Results

Thirty-two patients met the inclusion criteria. Three patients with recurrent tumors were excluded. Another seven patients were excluded due to artifacts. As a result, 22 patients (12 males and 10 females; age range, 42–83 years; median age, 66 years) with 22 tumors (21 glioblastomas [IDH-wildtype] and 1 anaplastic oligodendroglioma [IDH-mutant and 1p/19q-codeleted]) were finally included in the analysis.

Observers 1 and 2 placed 77 and 76 ROIs, respectively. Table 1 shows the mean and standard deviation values of each parameter obtained by the two observers.

Correlations between diffusion and perfusion parameters and APTSI. Table 2 summarizes the results of the correlation analysis. The two observers showed highly concordant results. For both observers, moderate positive correlations were observed between APTSI and ADC ($\rho = 0.625$ and $\rho = 0.490$ for observers 1 and 2, respectively; $p < 0.001$ for both). In addition, weak to moderate negative correlations were found between

	n	APTSI (%)	ADC ($\times 10^{-3}$ mm^2/s)	rCBV	K^{trans} ($\times 10^{-3}$ / min)	k_{ep} ($\times 10^{-3}$ /min)	v_e ($\times 10^{-3}$)	v_p ($\times 10^{-3}$)
Observer 1	77	3.01 ± 0.87	1.09 ± 0.24	3.92 ± 2.33	40.00 ± 18.23	238.23 ± 125.69	246.60 ± 223.17	13.72 ± 8.85
Observer 2	76	2.96 ± 0.88	1.07 ± 0.22	3.81 ± 2.22	42.49 ± 28.61	250.94 ± 130.86	235.89 ± 205.66	14.63 ± 12.12

Table 1. Mean values of quantitative MR imaging parameters.

	APTSI	ADC	K^{trans}	k_{ep}	v_e	v_p	rCBV
APTSI	1.000	0.625/0.490	0.139/0.099	− 0.454/− 0.397	0.387/0.334	− 0.248/− 0.201	− 0.141/− 0.168
	–	< 0.001/< 0.001	0.229/0.396	< 0.001/< 0.001	0.001/0.003	0.029/0.082	0.221/0.146
ADC		1.000	0.224/0.188	− 0.397/− 0.237	0.412/0.334	− 0.219/− 0.198	− 0.051/0.045
		–	0.050/0.104	< 0.001/0.039	< 0.001/0.003	0.056/0.086	0.658/0.700
K^{trans}			1.000	− 0.211/− 0.135	0.699/0.692	0.476/0.574	0.096/0.375
			–	0.066/0.244	< 0.001/< 0.001	< 0.001/< 0.001	0.406/0.001
k_{ep}				1.000	− 0.807/− 0.738	0.451/0.443	0.607/0.522
				–	< 0.001/< 0.001	< 0.001/< 0.001	< 0.001/< 0.001
v_e					1.000	− 0.066/0.020	− 0.378/− 0.160
					–	0.570/0.866	0.001/0.167
v_p						1.000	0.584/0.692
						–	< 0.001/< 0.001
rCBV							1.000
							–

Table 2. Correlations between quantitative MR imaging parameters. In each cell, numbers in upper and lower indicate Spearman's correlation coefficients (observer 1/observer 2) and corresponding p values (observer 1/observer 2), respectively.

	Standardized β	B	95% CI of B	P
ADC	0.585/0.476	2.093/1.877	1.423 to 2.763/1.071 to 2.683	< 0.001/< 0.001
K^{trans}	− 0.033/0.009	− 0.002/0.000	− 0.010 to 0.007/− 0.006 to 0.007	0.726/0.935
k_{ep}	− 0.232/− 0.202	− 0.002/− 0.001	− 0.003 to 0.000/− 0.003 to 0.000	0.047/0.075
CBV	0.084/− 0.104	0.031/− 0.041	− 0.048 to 0.110/− 0.131 to 0.048	0.434/0.359

Table 3. Multiple regression analysis examining associations between APTSI and diffusion/perfusion imaging parameters. Values for observer 1/observer 2 are shown for each item.

APTSI and k_{ep} ($\rho = -0.454$ and $\rho = -0.397$ and $p < 0.001$ for both) and between APTSI and v_e ($\rho = 0.387$ and $\rho = 0.334$ and $p = 0.001$ and $p = 0.003$ for observers 1 and 2, respectively). A weak negative correlation between APTSI and v_p ($\rho = -0.248$; $p = 0.029$) was found only by observer 1. No other parameters showed significant correlations with APTSI ($p > 0.05$). Multiple regression analysis (Table 3) revealed that ADC was significantly associated with APTSI ($p < 0.001$ for both observers), while k_{ep} was marginally associated with APTSI only for observer 1 ($p = 0.047$). No other parameters were significantly associated with APTSI ($p > 0.05$). Figure 2 shows relationships between APTSI and ADC for observers 1 and 2.

Correlations between diffusion and perfusion parameters. For both observers, ADC was significantly positively correlated with v_e ($\rho = 0.412$ and $\rho = 0.334$ and $p < 0.001$ and $p = 0.003$ for observers 1 and 2, respectively) and significantly negatively correlated with k_{ep} ($\rho = -0.397$ and $\rho = -0.237$ and $p < 0.001$ and $p = 0.039$, respectively). K^{trans} was significantly positively correlated with v_e ($\rho = 0.699$ and $\rho = 0.692$ for observers 1 and 2, respectively, and $p < 0.001$ for both) and v_p ($\rho = 0.476$ and $\rho = 0.574$ for observers 1 and 2, respectively, and $p < 0.001$ for both). k_{ep} was significantly positively correlated with v_p ($\rho = 0.451$ and $\rho = 0.443$ for observers 1 and 2, respectively, and $p < 0.001$ for both) and rCBV ($\rho = 0.607$ and $\rho = 0.522$ for observers 1 and 2, respectively, and $p < 0.001$ for both) and significantly negatively correlated with v_e ($\rho = -0.807$ and $\rho = -0.738$ for observers 1 and 2, respectively, and $p < 0.001$ for both). Finally, v_p was significantly positively correlated with rCBV ($\rho = 0.584$ and $\rho = 0.692$ for observers 1 and 2, respectively, and $p < 0.001$ for both).

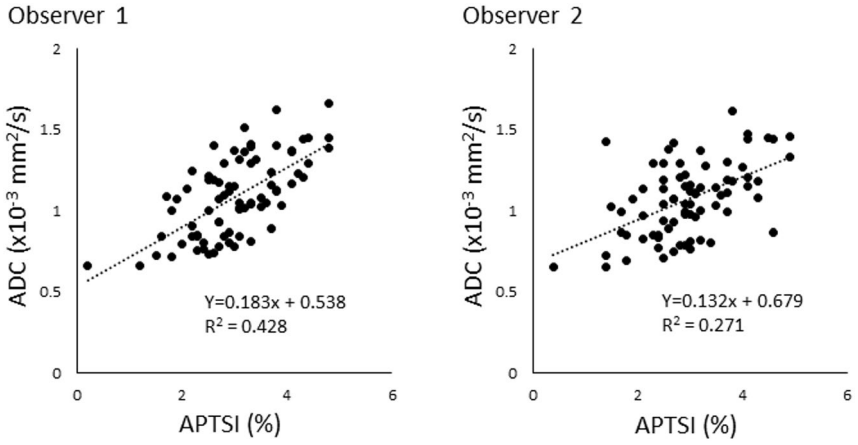

Figure 2. Scatter plots showing the relationships between APTSI and ADC for observers 1 and 2.

Discussion

Our results revealed a significant positive correlation between APTSI and ADC in ROIs within enhancing solid components of high-grade gliomas. To the best of our knowledge, no previous study has investigated the region-wise correlations between APTSI and other quantitative MRI parameters in malignant gliomas. The positive correlation between APTSI and ADC indicates that high APTSIs tend to originate in tissues with less diffusion restriction. The ADC has been linked with cell density in tumors: a significant negative correlation between ADC and histopathological cell density has been reported in several studies[18,19]. Thus, the positive correlation between APTSI and ADC in the results of this study seems inconsistent with the hypothesis that increased APTSI in high-grade gliomas originates from increased intracellular proteins and peptides in proliferating tumor cells. Recent studies have suggested contribution of extracellular proteins to ADC in glioblastoma. Pope et al.[20] reported overexpression of various proteins in the extracellular matrix (ECM) in glioblastomas that had higher ADC in the enhancing area than those with lower ADC. Patel et al.[21] reported overproduction of decorin in ECM in glioblastomas with higher ADC in the enhancing area. Decorin modulates the rigidity and stiffness of the ECM by binding with various ECM macromolecules and activating specific matrix metalloproteinases[22], which may in turn increase fluid mobility within the extracellular environment. These protein overproduction and molecular changes in ECM may increase mobile proteins and peptides in ECM that generate APT-related signal.

Mobile proteins in microscopic necrotic foci and fluid collection in microcysts can be another candidates for the concurrent increase of ADC and APTSI. Togao et al.[5] reported that gliomas with intratumoral microscopic necrosis show higher ATPSIs than those without microscopic necrosis.

A weak to moderate positive correlation was observed between APTSI and k_{ep}. We assume that this is due to the confounding effect of the moderate positive correlation between ADC and v_e, which showed a strong negative correlation with k_{ep}.

Our results do not exclude the intracellular origin of APTSI in brain tumors. Note that this study included only high-grade gliomas. Moreover, our ROIs only covered enhancing solid components. A well-documented APTSI increase from low-grade to high-grade gliomas may be related to the increasing intracellular cytosolic protein; a cohort of mixed low-grade and high-grade gliomas has shown a significant positive correlation between APTSI and cell density[5,6]. We are aware that the contribution of extracellular proteins and peptides should be evaluated with caution. Extracellular pH tends to be acidic due to lactate removal from the cell, which could result in lowered APTSI through reduction of amide proton exchange rate[23]. Thus, the contribution of extracellular proteins and peptides may not be large. In addition, our results do not reject the use of APTSI as an imaging marker for malignancy and the viability of tumors.

We did not find a significant correlation between APTSI and rCBV. The blood is rich in proteins and peptides, and studies have shown that intravascular blood can generate high APTSIs[24,25]. High-grade gliomas have high blood volume resulting from a rich neovascularization stimulated by vascular endothelial growth factor. Nonetheless, our results suggest that the blood in a tumor is not a dominant factor contributing to APTSI in high-grade gliomas.

The significant positive correlations between K^{trans} and v_e and between K^{trans} and v_p found in this study conform to the findings of a study by Mills et al.[26] and may represent a concurrent progression of tumor vascularization and permeability and the development of necrosis with tumor growth[27]. The significant positive correlation between rCBV and v_p, which is the blood plasma volume per unit volume of tissue, was predictable.

This study has several limitations. First, this is a retrospective study involving only 22 tumors from a single institution, which may have resulted in unknown biases. A prospective study with a larger sample size is needed to confirm the findings of this study. Second, our study population consisted predominantly of glioblastomas, IDH-wildtype. Although glioblastoma, IDH-wildtype is the most common type of high-grade glioma, our findings may not be applicable to other types of high-grade gliomas. Third, the non-enhancing components of the tumors were excluded from the analyses. We included only enhancing components because in high-grade gliomas, distinguishing tumor invasion from vasogenic edema in the non-enhancing T2-prolonged areas surrounding

the enhancing tumor is often difficult. Fourth, APT imaging was performed using a single-slice sequence, which limited the volume coverage. Finally, the two observers freely placed the ROIs using post-contrast images as guidance. Thus, the inter-observer reproducibility of their results could not be quantified using a statistical index. Nonetheless, their results were in close agreement.

Conclusion

The APTSI in the enhancing component was positively correlated with ADC in high-grade gliomas. Extracellular proteins and peptides may be contributors to high APTSI in high-grade gliomas. Further studies are needed to elucidate their roles in APTSI in high-grade gliomas.

Data availability

The datasets generated and/or analyzed during this study are available from the corresponding author upon reasonable request.

Received: 28 January 2021; Accepted: 18 May 2021
Published online: 27 May 2021

References

1. Ward, K. M., Aletras, A. H. & Balaban, R. S. A new class of contrast agents for MRI based on proton chemical exchange dependent saturation transfer (CEST). *J. Magn. Reson.* **143**, 79–87 (2000).
2. Zhou, J., Payen, J. F., Wilson, D. A., Traystman, R. J. & van Zijl, P. C. Using the amide proton signals of intracellular proteins and peptides to detect pH effects in MRI. *Nat. Med.* **9**, 1085–1090 (2003).
3. Zhou, J., Lal, B., Wilson, D. A., Laterra, J. & van Zijl, P. C. Amide proton transfer (APT) contrast for imaging of brain tumors. *Magn. Reson. Med.* **50**, 1120–1126 (2003).
4. Jones, C. K. *et al.* Amide proton transfer imaging of human brain tumors at 3T. *Magn. Reson. Med.* **56**, 585–592 (2006).
5. Togao, O. *et al.* Amide proton transfer imaging of adult diffuse gliomas: Correlation with histopathological grades. *Neuro Oncol.* **16**, 441–448 (2014).
6. Sakata, A. *et al.* Diagnostic performance between contrast enhancement, proton MR spectroscopy, and amide proton transfer imaging in patients with brain tumors. *J. Magn. Reson. Imaging* **46**, 732–739 (2017).
7. Zhou, J. *et al.* Differentiation between glioma and radiation necrosis using molecular magnetic resonance imaging of endogenous proteins and peptides. *Nat. Med.* **17**, 130–134 (2011).
8. Park, K. J. *et al.* Added value of amide proton transfer imaging to conventional and perfusion MR imaging for evaluating the treatment response of newly diagnosed glioblastoma. *Eur. Radiol.* **26**, 4390–4403 (2016).
9. Mehrabian, H., Desmond, K. L., Soliman, H., Sahgal, A. & Stanisz, G. J. Differentiation between radiation necrosis and tumor progression using chemical exchange saturation transfer. *Clin. Cancer Res.* **23**, 3667–3675 (2017).
10. Sagiyama, K. *et al.* In vivo chemical exchange saturation transfer imaging allows early detection of a therapeutic response in glioblastoma. *Proc. Natl. Acad. Sci. U. S. A.* **111**, 4542–4547 (2014).
11. Joo, B. *et al.* Amide proton transfer imaging might predict survival and IDH mutation status in high-grade glioma. *Eur. Radiol.* **29**, 6643–6652 (2019).
12. Wen, Z. *et al.* MR imaging of high-grade brain tumors using endogenous protein and peptide-based contrast. *Neuroimage* **51**, 616–622 (2010).
13. Jeong, H. K. *et al.* Characterizing amide proton transfer imaging in haemorrhage brain lesions using 3T MRI. *Eur. Radiol.* **27**, 1577–1584 (2017).
14. Keupp, J., Baltes, C., Harvey, P. R. & Van den Brink, J. Parallel RF transmission based MRI technique for highly sensitive detection of amide proton transfer in the human brain at 3T. *Proc. Int. Soc. Magn. Reson. Med.* **19**, 710 (2011).
15. Togao, O. *et al.* Scan-rescan reproducibility of parallel transmission based amide proton transfer imaging of brain tumors. *J. Magn. Reson. Imaging* **42**, 1346–1353 (2015).
16. Shen, Y. *et al.* T1 relaxivities of gadolinium-based magnetic resonance contrast agents in human whole blood at 1.5, 3, and 7T. *Investig. Radiol.* **50**, 330–338 (2015).
17. Thévenaz, P., Ruttimann, U. E. & Unser, M. A pyramid approach to subpixel registration based on intensity. *IEEE Trans. Image Process.* **7**, 27–41 (1998).
18. Iima, M. *et al.* Characterization of glioma microcirculation and tissue features using intravoxel incoherent motion magnetic resonance imaging in a rat brain model. *Investig. Radiol.* **49**, 485–490 (2014).
19. Kinoshita, M. *et al.* Comparison of diffusion tensor imaging and 11C-methionine positron emission tomography for reliable prediction of tumor cell density in gliomas. *J. Neurol. Surg.* **125**, 1136–1142 (2016).
20. Pope, W. B. *et al.* Differential gene expression in glioblastoma defined by ADC histogram analysis: Relationship to extracellular matrix molecules and survival. *AJNR Am. J. Neuroradiol.* **33**, 1059–1064 (2012).
21. Patel, K. S. *et al.* Decorin expression is associated with predictive diffusion MR phenotypes of anti-VEGF efficacy in glioblastoma. *Sci. Rep.* **10**, 14819 (2020).
22. Jarvelainen, H., Sainio, A. & Wight, T. N. Pivotal role for decorin in angiogenesis. *Matrix Biol.* **43**, 15–26 (2015).
23. Zhou, J., Heo, H. Y., Knutsson, L., van Zijl, P. C. M. & Jiang, S. APT-weighted MRI: Techniques, current neuro applications, and challenging issues. *J. Magn. Reson. Med.* **50**, 347–364 (2019).
24. Zheng, S. K. *et al.* Chemical exchange saturation transfer effect in blood. *Magn. Reson. Med.* **71**, 1082–1092 (2014).
25. Bohara, M., Kamimura, K., Nakajo, M., Yoneyama, T. & Yoshiura, T. Amide proton transfer imaging of cavernous malformation in the cavernous sinus. *Magn. Reson. Med. Sci.* **18**, 109–110 (2019).
26. Mills, S. J. *et al.* Extravascular extracellular space derived from dynamic contrast-enhanced MR imaging. *AJNR Am. J. Neuroradiol.* **37**, 811–817 (2016).
27. Pike, M. M. *et al.* High-resolution longitudinal assessment of flow and permeability in mouse glioma vasculature: Sequential small molecule and SPIO dynamic contrast agent MRI. *Magn. Reson. Med.* **61**, 615–625 (2009).

Acknowledgements

We thank Dr. Chihaya Koriyama for her assistance in statistical analysis.

Author contributions

T.Y. designed the study. M.N., M.B., K.K., and N.H. performed the data collection and preprocessing. Moreover, M.N., M.B., and K.K. performed the data analysis and interpretation. The manuscript was written by M.B. and T.Y. and reviewed by all authors.

Competing interests

The authors declare no competing interests.

Additional information

Supplementary Information The online version contains supplementary material available at https://doi.org/10.1038/s41598-021-90841-z.

Correspondence and requests for materials should be addressed to T.Y.

Reprints and permissions information is available at www.nature.com/reprints.

Publisher's note Springer Nature remains neutral with regard to jurisdictional claims in published maps and institutional affiliations.